1 **The Effect of the Wenchuan and Lushan Earthquakes on the Size**

2 **Distribution of Earthquakes along the Longmenshan Fault**

3 Chun Hui[1,2,3], Changxiu Cheng[1,2,3,4*], Shi Shen[1,2,3], Peichao Gao[1,2,3], Jin Chen[1,2], Jing Yang[5], Min

4 Zhao[1,2,3]

5 [1] Key Laboratory of Environmental Change and Natural Disaster, Beijing Normal University, China,

6 100875

7 [2] State Key Laboratory of Earth Surface Processes and Resource Ecology, Beijing Normal

8 University, China, 100875

9 [3] Faculty of Geographical Science, Center for Geodata and Analysis, Beijing Normal University,

10 China, 100875

11 [4] National Tibetan Plateau Data Center, Beijing, China, 100101

12 [5] College of Data Science, Taiyuan University of Technology, China, 030024

14 Corresponding author: Changxiu Cheng

19
20
21
22
23
24
25
26
27
28
29
30
31
32

Abstract

Changes in the stress state of faults and their surroundings is a highly plausible mechanism explaining earthquakes interaction. These stress changes can impact the seismicity rate and the size distribution of earthquakes. However, the effect of large earthquakes on the earthquake size distribution along the Longmenshan fault has not been quantified. We evaluated the levels of the b value for the stable state before and after the large earthquakes on 12 May 2008 (Wenchuan, M_S 8.0) and 20 April 2013 (Lushan, M_S 7.0) along the Longmenshan fault. We found that after the mainshocks, the size distribution of the subsequent earthquakes shifted toward relatively larger events in the Wenchuan aftershock zone (b value decreased from 1.03 to 0.84), and generally remained invariable in the Lushan aftershock zone (b value remained at 0.76). The time required for the b value to return to stable states after both mainshocks were entirely consistent with the time needed by the aftershock depth images to stop visibly changing. The result of the temporal variation of b values show decreasing trends for the b value before both large earthquakes. Our results are available for assessing the potential seismic risk of the Longmenshan fault as a reference.

Keywords: b value; stable state; depth; Longmenshan fault

1 Introduction

Following the Wenchuan M_S 8.0 earthquake on 12 May 2008, the Longmenshan fault zone was struck by the 20 April 2013 M_S 7.0 Lushan earthquake. The Longmenshan fault zone is composed of several almost parallel thrust faults, forming a boundary fault between the Sichuan Basin and Tibetan Plateau, and controls the seismicity of the Longmenshan region (Fig. 1). The epicenters of the Wenchuan and Lushan earthquakes were approximately 87 km apart, and the focal mechanism of both events showed a thrust rupture (Jia et al., 2014).

According to the characteristics of the Wenchuan and Lushan earthquakes, whether the M_S 7.0 Lushan event was a strong aftershock of the M_S 8.0 Wenchuan earthquake or a new and independent event has been a topic of debate. For example, some researchers suggest that the two large earthquakes were independent events. The reasons are as follows: (1) there is no overlapping area between the Wenchuan and Lushan earthquake rupture zones (Zhang et al., 2013); (2) the Wenchuan and Lushan earthquakes were generated in different faults in the Longmenshan fault zone (Li et al., 2014); (3) the rupture processes of the Wenchuan and Lushan earthquakes were different, and the aftershock zones of the two events were nearly 45 km apart (Du et al., 2013). Alternatively, some scientists propose that the Wenchuan and Lushan earthquakes were a mainshock-aftershock sequence and note that the Lushan event struck in an area where Coulomb stress was increased due to the Wenchuan earthquake (Parsons and Segou, 2014; Zhu, 2016).

The controversy over the relationship between the Wenchuan and Lushan earthquakes highlights the complexity of earthquakes interaction in the Longmenshan fault zone. It is widely accepted that earthquakes interactions can be understood by identifying changes in static and dynamic stress states around faults (Toda et al., 2011; Wedmore et al., 2017; Verdecchia et al., 2018).

71 The most observable effect of this stress change is a significant increase in seismicity rate, which is
72 generally considered an aftershock phenomenon (Kilb et al., 2002; Toda et al., 2012; Devries et al.,
73 2018). Statistically, aftershock activity is classically described by $n(t) = K/(t + c)^p$, where $n(t)$ is the
74 number of aftershocks after time t and K, c, and p are constants that describe the aftershock
75 productivity (Utsu et al., 1995). Ogata (1988,1998) described aftershock activity as a
76 multigenerational branching process and proposed the epidemic-type aftershock sequence model,
77 which is a stochastic point process model of self-exciting point processes.

78 Changes in stress can impact the seismicity rate and the frequency size distribution, which is
79 alternatively known as the frequency-magnitude distribution (FMD) (Gulia et al.,2018) or
80 Gutenberg-Richter (G-R) law (Gutenberg and Richter,1944) and is expressed as $logN=a-bM$, where
81 N is the number of events in a given time period with magnitude greater than M, a describes the
82 seismicity of a volume, and b is slope of the FMD. Previous studies showed that b values fall within
83 the range of 1.02 ± 0.03 on a large scale for a long time (Wech et al., 2010; El-Isa et al., 2014). For
84 regions on a smaller scale, the b values show a broad range of spatial and temporal variations. For
85 example, the b value ranged from 0.5 to 2.5 in the Andaman–Sumatra region and California
86 (Nuannin et al., 2005). Interpretation of the variation of b values is based on several factors,
87 including stress state (Amitrano, 2003; Goebel et al., 2013), focal depth (Spada et al., 2013), faulting
88 style (Schorlemmer et al., 2005; Gulia et al. 2010), fluid pressure (Bachmann et al., 2012), and so
89 on.

90 The earthquake size distribution generally follows a power law, with a slope of b values, which
91 characterizes the relative occurrence of large and small events. A low b value indicates a larger
92 proportion of large earthquakes and vice versa. Zhao et al. (2008) compared the spatial footprint of
93 b values before and after the Wenchuan earthquake in the Longmenshan fault zone, and the results
94 showed that the b values tend to change from lower in the southern region to higher in the
95 northeastern region. The temporal change in b values before the Wenchuan M_S 8.0 earthquake
96 showed a decreasing trend (Zhang et al., 2016; Liu et al., 2017; Shi et al., 2018), and the Lushan M_S
97 7.0 earthquake showed similar temporal change trends in b values (Zhao et al., 2020). These studies
98 focused on the variation trend of b values before and after the two large events along the
99 Longmenshan fault. However, the fundamental effect of the Wenchuan and Lushan earthquakes on
100 the size distribution of earthquakes along the Longmenshan fault has not been quantified, which
101 limits our understanding of how the apparent stress changes in the region affect the size distribution
102 of earthquakes.

103 In this study, we evaluated the spatiotemporal evolution of the b values along the Longmenshan
104 fault in the past nearly 20 years. Moreover, we estimated the levels of the b value for the stable state
105 before and after the Wenchuan and Lushan earthquakes and quantified the effects of the two large
106 earthquakes on the size distribution of subsequent events at different times. In addition, the spatial
107 evolution process of the deep seismogenic environment in the Wenchuan and Lushan aftershock
108 zones in two and three dimensions was illustrated via spatial scanning and data fitting, which can
109 be used to analyze the aftershock activity of the two large earthquakes.

110
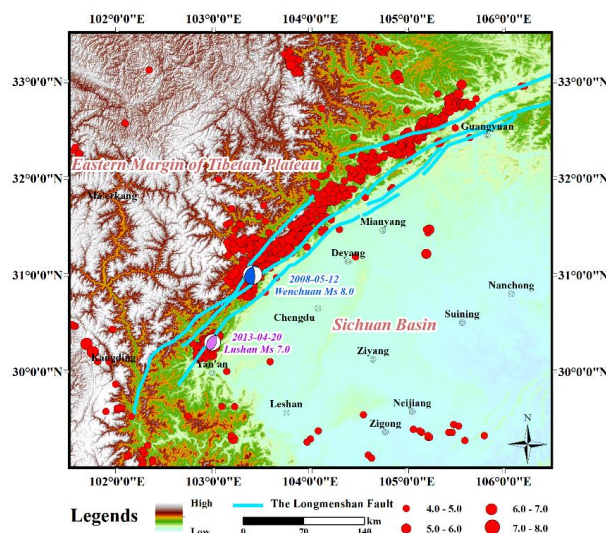
Figure 1. The topographic and tectonic map of the Longmenshan fault zone and its surrounding region.

Blue beach ball represents the focal mechanism of the Wenchuan M_S 8.0 earthquake. Pink beach ball represent the

focal mechanism of the Lushan M_S 7.0 earthquake. Red circles represent epicenters of earthquakes (Ms≥4) from 1

January 2000 to 1 January 2019.

2 Data and Postulates

The earthquake catalog we used here was documented by the regional seismic network and
then verified by the China Earthquake Networks Center (CENC) along the Longmenshan fault
during the period from 1 January 2000 to 1 January 2019. It is a relatively complete catalog
containing the Wenchuan-Lushan earthquake sequence.

Figure 2 shows the magnitude-time distribution of earthquakes in the Wenchuan source region
and Lushan source region. The locations of the earthquakes in this catalog were corrected for
accuracy. Each event includes the time, location, magnitude and depth. Homogeneity of the catalog
was iterated and optimized for subsequent research and analysis.

124
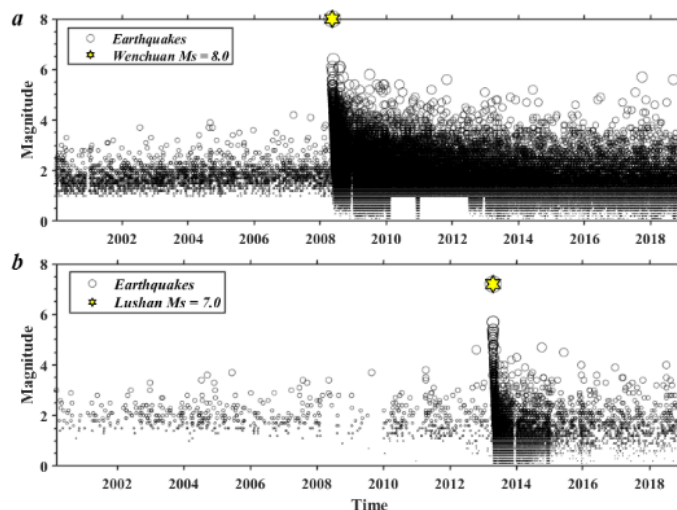
Figure 2. Magnitude versus time for events in the Longmenshan fault zone from 2000 to 2019.

a Magnitude versus time for events in the M_S 8.0 Wenchuan source region; **b** Magnitude versus time for

events in the M_S 7.0 Lushan source region

Stress change has been widely used to interpret the triggering of the mainshock-mainshock and mainshock-aftershock events (Stein et al., 1997; Mallman and Zoback, 2007; Toda et al., 2011; Delescluse et al., 2012; Durand et al., 2013; Sumy et al., 2014). However, the exact measurement of stress states is difficult; thus, a relationship between the stress state and b value has been proposed (Zuniga and Wyss, 2001; Schorlemmer et al., 2005; Nanjo et al., 2012; Gulia et al.,2018). Schorlemmer et al. (2005) demonstrated that the b value could be regarded as a stress indicator that depends inversely on differential stress. Therefore, changes in the stress state on faults lead to the variation in b values, which is followed by time-dependent recovery. In general, the larger the magnitude of the earthquake, the greater the stress changes and the larger the b value fluctuations. No event of magnitude larger than M 7.0 had been reported in the historical record of the Longmenshan fault zone and the catalog we used in this paper contains more than 80,000 events and only two large earthquakes greater than magnitude 6.5, that is, the Wenchuan M_S 8.0 and Lushan M_S 7.0 earthquakes. Thus, these two events are mainly responsible for the apparent changes in stress state along the Longmenshan fault zone in the past 20 years.

Therefore, there are two postulates: first, without a large earthquake perturbation, the b value will remain in a stable state with a small fluctuation range for a long time; second, after the perturbation of a large earthquake, the b value may recover to another stable state. We evaluated the levels of the b value for the stable state before and after these two large earthquakes in the study region.

3 Methods

The main methods we used include estimation methods (MaxCurvature for the estimation of the completeness magnitude; maximum likelihood estimation (MLE) for the b value estimation),

150   test methods (Akaike information criterion (AIC) for the variation trend of b values; the nonlinearity

151   index (NLIndex) for the linearity assessment of frequency-magnitude distribution) and kriging

152   interpolation to describe the spatial and temporal evolution images of aftershock focal depth.

153   3.1 Completeness magnitude (M_C) and b value estimation

154   The estimation of the completeness of earthquake catalogs is essential to the computation of b

155   values, and the lowest magnitude of all earthquakes that are reliably detected in a space-time volume

156   is defined as the completeness magnitude (M_C) (Woessner and Wiemer,2005). The lower the M_C,

157   the higher the detection capability. Here, we use the MaxCurvature technique, which estimates the

158   M_C by locating the magnitude that is the highest frequency of events in the FMD. Mignan (2011)

159   showed that the MaxCurvature technique underestimates the M_C in cases involving gradually curved

160   FMDs and postulated that this underestimation tendency arises from spatiotemporal heterogeneities

161   within the earthquake monitoring network. Therefore, we used the corrected MaxCurvature method

162   with a correction factor of +0.2 (Gulia and Wiemer, 2019), and the uncertainties were determined

163   by bootstrapping.

164   The least-squares method and maximum likelihood estimation are often used to calculate the

165   b value, and the latter approach is considered more stable. In this work, the maximum likelihood

166   estimation used to calculate the b value and its standard deviation (Aki, 1965; Utsu, 1965):

167
$$b = \frac{1}{\ln(10)(\overline{M} - M_C)}$$

168   where $\overline{M}$ is the average magnitude of earthquakes with $M \geq M_C$; M_C is the cutoff magnitude. The

169   confidence limit of the b value is expressed as follows:

170
$$\sigma = \frac{b}{\sqrt{N}}$$

171   where N is the number of earthquake cases of the given sample.

172   3.2 Estimation of the frequency-magnitude distribution (FMD) extrapolation

173   The nonlinearity index (NLIndex) can be used to assess whether the extrapolation of a given

174   high-magnitude FMD is likely an overestimate or underestimate of the probable rates for large

175   events (Tormann et al., 2014).

176   1)   Calculate the b value for all Mcut from Mcmin to the highest Mcut for which Nmin events

177   are still sampled.

178   2)   Divide the standard deviation by the largest individual b value uncertainty for each

179   possible Mcut, and for each Mcut, this value is the NLIndex.

180   3)   Divide the NLIndex for each Mcut by the number of estimated b values to weight the result

181   by data density.

182   4)   Find the minimum weighted NLIndex to find the best M_C that produces the most linear

183   FMD fit.

184   If NLIndex $\leq$ 1, the FMD is regarded as linear, and if NLIndex > 1, the FMD is not linear. The

185   slope of Mcut is clearly positive or negative, respectively indicating that the FMD overestimates

186   or underestimates large M rates.

187   3.3 Akaike information criterion

188   To quantify the changing trend of b values, the P test was conducted for b values in two sample

189   windows based on the Akaike information criterion (AIC) (Akaike, 1974). Hypothesis 1: the b

190   values in the two sample windows are the same; Hypothesis 2: the b values in the two sample
191   windows are different, respectively represented as b_1 and b_2. The hypothesis of the difference of the
192   AIC leads to the difference ΔAIC (Utsu,1992):

$$\Delta AIC = -2(N_1 + N_2)\ln(N_1 + N_2) + 2N_1\ln(N_1 + \frac{N_2 b_1}{b_2}) + 2N_2\ln(N_2 + \frac{N_1 b_2}{b_1}) - 2$$

194   where N_i is the numbers of events in the sample windows and b_i is b values in the sample windows.
195   P_b represents the probability that the events in the two sample windows come from the same
196   population and can be derived from the AIC as follows:

$$P_b = e^{(-\Delta AIC/2)-2}$$

198   The b value in the sample window represents a significant change when $\Delta AIC \geq 2$ ($P_b \approx 0.05$) and is
199   highly significant when $\Delta AIC > 5$ ($P_b \approx 0.01$) (Utsu, 1999).
200

201   3.4 Kriging interpolation
202   Kriging interpolation is the most commonly used geostatistical approach for spatial
203   interpolation. With this method, a semivariogram is used to express the spatial relationship of the
204   distance between samples. This technique depends on the spatial model between samples to predict
205   attribute values at unsampled locations (McGrath et al. 2004). As a widely used interpolation
206   method, kriging takes into account the distance between unknown positions and the sample
207   locations as well as the distance between sample locations, effectively reducing the interference of
208   clustering in samples on the accuracy of the interpolated estimates (Ha et al., 2014). We used the
209   kriging interpolation algorithm to produce maps incorporating anisotropy and underlying trends
210   from irregularly spaced data.
211   The exponential semivariance model with the smallest prediction errors was chosen over the
212   Gaussian and spherical models for the spatial interpolation of focal depth data.

213   **4 Results and Analysis**

214   4.1 Completeness magnitude (M_C) and linearity assessment of frequency-magnitude
215   distribution (FMD)
216   As shown in Fig. 3, the results of the corrected MaxCurvature method show that the M_C of the
217   earthquake catalog used in this work is M_C=1.5. This result is consistent with the results of previous
218   studies on the Wenchuan earthquake zone (Huang, 2008; Shi et al.,2018). Fang et al. (2015)
219   described in detail the aftershock performance and analysis of the Lushan earthquake based on the
220   combined data from permanent and temporary seismic stations. They concluded that the minimum
221   complete magnitude was M=1.0. To unify the consistency of the M_C of the Wenchuan M_S 8.0 and
222   Lushan M_S 7.0 earthquakes in the Longmenshan fault zone, we selected events with magnitudes of
223    $M \geq M_C$=1.5.
224   We performed a linearity check on FMD, and the results are shown in Fig. 4. The NLIndex
225   (red) is shown for different cutoff magnitudes (upper inset) and the NLIndex ≤ 1 for all cut off
226   magnitudes; thus, the linear FMD is accepted as the best M_C.
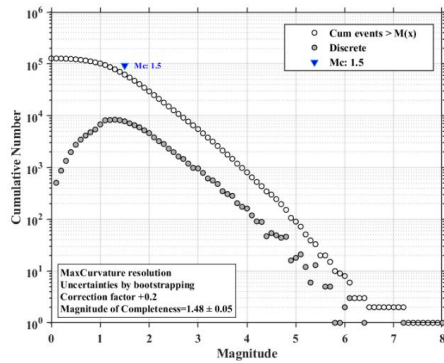
Figure 3. Frequency-magnitude distribution of the seismicity of the Wenchuan-Lushan sequence from 1 January 2000 to 1 January 2019
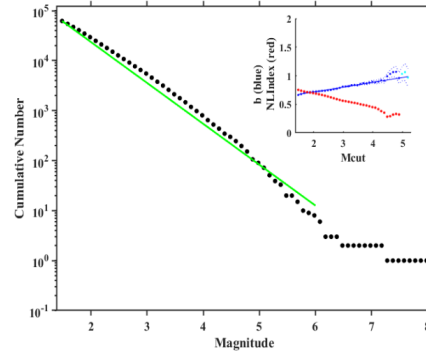
Figure 4. Frequency-magnitude distribution and NLIndex.

227   4.2 Time-space analysis of b values

228   Earthquake frequency will increase immediately within a short time after a large event and
229   may exceed the recording capacity of the seismic network. Before establishing the time-space series
230   of b values with aftershocks, we should eliminate the events documented in the early catalog, which
231   is somewhat heterogeneous and incomplete in small events (Gulia and Wiemer, 2019). In this work,
232   the exclusion period depends on the magnitude of completeness over time. Therefore, we first
233   removed the events documented in the initial catalog within two months after the Wenchuan M_S 8.0
234   and Lushan M_S 7.0 earthquakes, a period for which the data are highly incomplete. Then, we
235   calculated the spatiotemporal distributions of b values before and after two large events that
236   occurred from 2000-2019 along the Longmenshan fault by selecting events with $M \geq M_C = 1.5$ and
237   using a time window and spatial grid to calculate the b values. In this computation, the window
238   lengths were set to at least 500 events in the Wenchuan aftershock zone and 200 events in the Lushan
239   aftershock zone. Each window was moved forward by one event at a time.

240   Figures 5a and 5b display time series of the b value in source regions, and the overall change
241   trend conforms to our postulation that b values will undergo relatively significant changes in a
242   period of time before and after a large earthquake. Specifically, b values show a decreasing trend
243   before the occurrence of both large earthquakes in both zones. To ensure that this trend is statistically
244   significant, we quantitatively assessed the temporal variation in b values using the P parameter test
245   and selected three windows before the M_S 8.0 event (W_1, $W_{2,}$ and W_3) and the M_S 7.0 event (L_1, $L_{2,}$
246   and L_3). Window selection was based on the significance of changes in b values (Fig. 5a, 5b). The
247   results are shown in Table 1. The b value in the sample window has significantly changed when
248    $\Delta AIC \geq 2$ ($P_b \approx 0.05$) (Utsu,1999). Table 1 shows that the b values decreased before both large
249   earthquakes with statistically significant variations.

250

251   **Table 1 Results of the P parameter test between windows**

Windows	ΔAIC	P_b
$W_1 \& W_2$	3.8	0.02
$W_2 \& W_3$	3.2	0.03
$W_1 \& W_3$	19.9	6.4×10^{-6}
$L_1 \& L_2$	2.6	0.03

$L_2 \, \& L_3$	4.6	0.01
$L_1 \, \& L_3$	20	5.9×10^{-6}

252   After the Wenchuan M_S 8.0 event, the b values in the Wenchuan aftershock zone experienced
253   a period of dramatic fluctuation (indicated by the pink shading lasting not more than one year)
254   before gradually stabilizing within a small fluctuation range (Fig. 5a), which was similar to the range
255   of b values in the third period (Fig. 5c, $b=0.84$). After the Lushan M_S 7.0 event, the b values in the
256   Lushan aftershock zones increased rapidly and then slowly dropped to a stable state (Fig. 5b), which
257   was similar to the FMD in the first period (Fig. 5d, $b=0.76$). As shown in Fig. 5b (red shading), the
258   b value required less than ten months to return to a stable state.

259   The reference b values can be estimated for the background levels (for the period, $b=1.03$ in
260   the Wenchuan aftershock zone and $b=0.76$ in the Lushan aftershock zone). When the perturbation
261   effect of the mainshocks gradually decreases, the b values in the Lushan aftershock zone eventually
262   return to the background level ($b=0.76$), whereas those in the Wenchuan aftershock zone drop below
263   the background level (from 1.03 to 0.84). To date, there have been no earthquakes that have
264   significantly changed the stability of the Longmenshan fault zone since the M_S 7.0 Lushan
265   earthquake.

266   The temporal distribution of earthquakes also indicates the change in stress state of faults and
267   their surroundings. As shown in Fig. 2a, before the M_S 8.0 Wenchuan earthquake, the frequency of
268   events in the Wenchuan aftershock zone had been decreasing for a year since 2006, and only two
269   events greater than M_S 4 occurred during the period when b values were significantly decreasing
270   (Fig. 5a). However, earthquakes greater than M_S 4 struck the entire Wenchuan aftershock zone after
271   the M_S 8.0 event (Fig. 1). In addition, there were no strong aftershocks above magnitude 6.5 along
272   the faults, and only six events greater than M_S 4 occurred within two months after the mainshock.
273   These phenomena indicate that without the continuous perturbation of strong aftershock, the b value
274   gradually stabilized to the state mainly determined by the background earthquakes, which tended to
275   shift to larger events following the M_S 8.0 event in the Wenchuan aftershock zone.

276   After the M_S 8.0 Wenchuan earthquake, the Lushan aftershock zone also experienced a
277   "seismic quiescence" of approximately two years, and only one event greater than M_S 4 occurred
278   before the M_S 7.0 Lushan earthquake during the period when b values were significantly decreasing
279   (Fig. 2b). Moreover, only a few events greater than M_S 4 occurred within two months after the
280   mainshock; the subsequent events basically returned to the magnitude of the background
281   earthquakes before the mainshock, which shows that the b values in the Lushan aftershock zone
282   eventually returned to the background level (Fig. 5b).
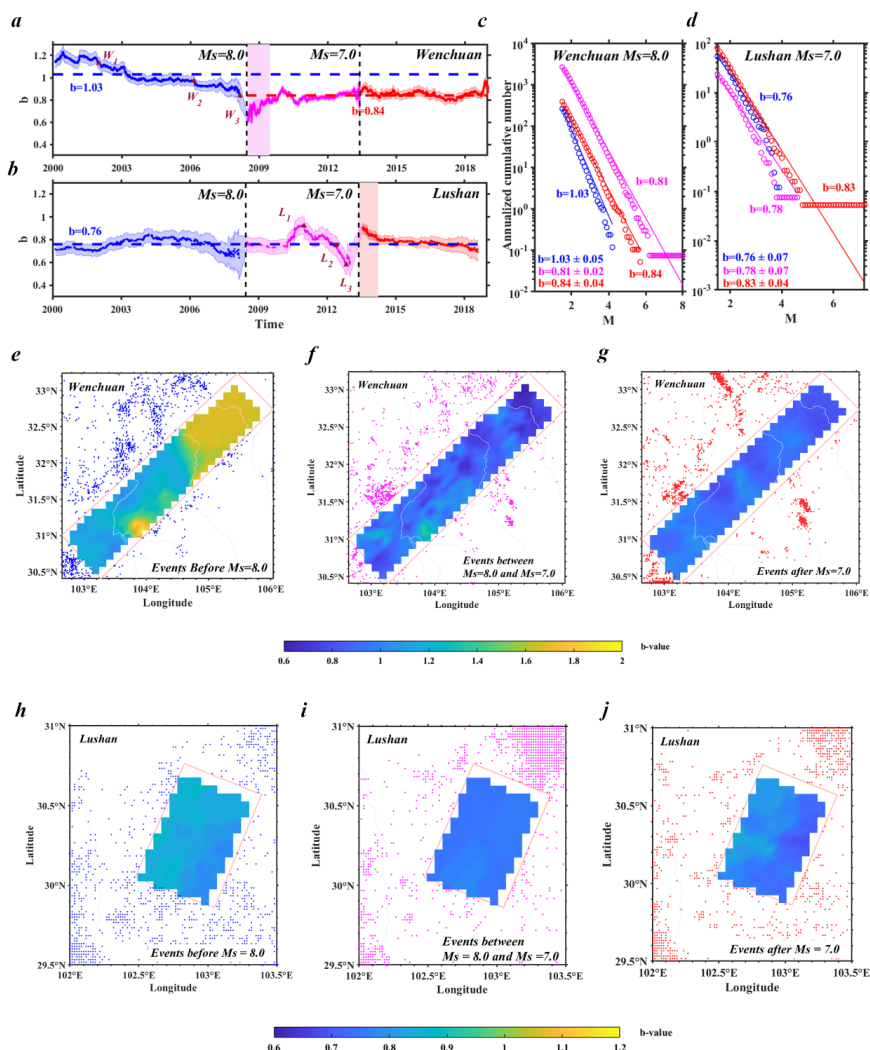
Figure 5. Temporal and spatial analysis of the *b* values for the Wenchuan-Lushan sequence

a, **b**, Temporal variation of *b* values for the Wenchuan and Lushan source regions. The dashed black lines represent the times of the M_S 8.0 (Wenchuan) and M_S 7.0 (Lushan) events, and the dashed blue lines show the background *b* values for the Wenchuan and Lushan source regions. The dashed red line represents the *b* value after the time of the M_S 7.0 event (Lushan) for the Wenchuan source region. The shaded regions represent the uncertainties in the *b* values. **c**, **d**, FMDs for the two aftershock zones in three different periods. **e**, **f**, **g**, Map showing the spatial footprint of *b* values for the Wenchuan aftershock zone in three different periods. **h**, **i**, **j**, Map showing the spatial footprint of *b* values for the Lushan aftershock zone in three different periods.

To analyze the spatial footprints of the changes in the *b* values, we divided the two study regions into 0.1°×0.1° grids, sampled the 300 events nearest to each grid node within radius of 30 km, and re-estimated the M_C in each node. For this purpose, we used a bootstrap approach to sample the events 1000 times randomly. The spatial footprints of the changes in the *b* values are consistent

296 with the FMDs (Fig. 5c, 5d). Figures 5e-5g demonstrate the spatial variation in the b values
297 throughout the Wenchuan aftershock zone. Figures 5h-5j show the spatial variation in the b values
298 in the Lushan aftershock zone.

299   The b value in the southern part of the Wenchuan source region and Lushan source region was
300 lower than that in the northern part of the Wenchuan aftershock before the M_S 8.0 Wenchuan event
301 (Fig. 5e, 5h). This pattern is consistent with the characteristics of the Longmenshan fault, which is
302 a strike-slip fault in the north and a thrust fault in the southern section. It is generally considered
303 that the b value is inversely proportional to stress, and the b values of different types of faults are as
304 follows: b(normal) > 1, b(strike-slip)~1, and b(thrust) < 1 (Schorlemmer et al., 2005; Gulia et al.
305 2010). The conditions changed markedly after the M_S 8.0 Wenchuan event; the b values decreased
306 in the Wenchuan source region and Lushan source region (Fig. 5f, 5i). This finding illustrates the
307 effect of the Wenchuan earthquakes on stress change along the Longmenshan fault. Figures 5g and
308 5j illustrate the stable state of the b value in the Longmenshan fault zone.

309 4.3 Evolution of images of aftershock activity depicted by focal depth

310   Spatial scanning was performed using events with depth data in the catalog, i.e., at a step size
311 of 0.1° for both longitude and latitude. For all earthquakes in each 0.1°×0.1° grid point, the average
312 depth was used as the depth value of the grid point, and then kriging interpolation was applied to all
313 the grids. We counted at least ten events in each grid node in the Wenchuan aftershock zone as
314 samples (as well as five events for the Lushan aftershock zone) to prevent the average depth of grid
315 points from being affected by too few events. The contour lines of depth distribution at different
316 periods after the mainshock were obtained and superimposed with regional faults (Fig. 6, Fig. 7).

317   To illustrate the evolution of the deep seismogenic environment in the Wenchuan aftershock
318 zone. Figure 6 shows the spatial evolution of the aftershock depth at one day, one week, one month,
319 six months, one year and three years after the mainshock. The analysis shows that the focal depth
320 of the Wenchuan aftershock zone spread along the direction of the fault. With Mianyang as the
321 boundary, the aftershock zone can be divided into the southern section and the northern section. The
322 depth distribution is generally deep in the southeast and shallow in the northwest, and the average
323 aftershock focal depth is 10-15 km.

324   A comparison of the aftershock activity images depicted by the focal depth information shown
325 in Fig. 6d and Fig. 6e revealed that the image formed one year after the mainshock did not show a
326 significantly different pattern in the following two years. This finding indicates that after the
327 mainshock, the aftershock frequency tends to be stable one year later, which means that the
328 aftershock active period of the Wenchuan M_S 8.0 was less than one year.

329   Figure 7 shows the spatial evolution of aftershock depths at one day, one week, five months,
330 ten months, one year and three years after the mainshock in the Lushan aftershock zone. The analysis
331 shows that the focal depths of the Lushan aftershock are distributed around the fault, with the fault
332 as the boundary, with a trend of deep in the southeast and shallow in the northwest. Moreover, a
333 comparison of the regional aftershock activity images depicted by the focal depth information in
334 Fig. 7d and Fig. 7e revealed that the pattern of the image formed ten months after the mainshock
335 presented limited changes in the following one year, which indicates that the aftershock frequency
336 tended to be stable ten months after the Lushan mainshock. Therefore, the aftershock active period
337 of the Lushan M_S 7.0 earthquake was less than ten months.
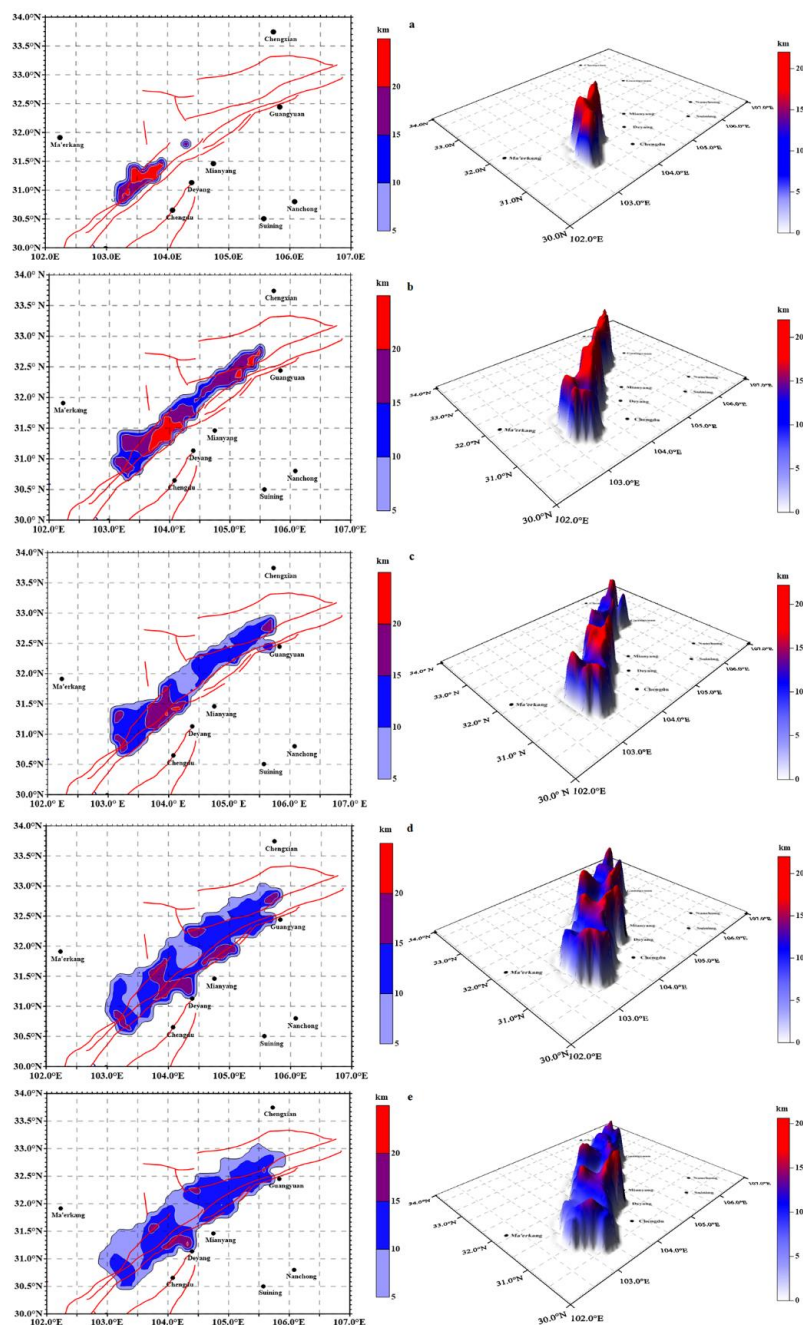
Figure 6. Spatial distribution of the focal depths of the aftershocks following the Wenchuan *Ms* 8.0 earthquake on the fault plane. Red lines represent the locations of faults. **a** One day after the mainshock; **b** 1 week after the mainshock; **c** 1 month after the mainshock; **d** 1 year after the mainshock; and **e** 3 years after the mainshock.
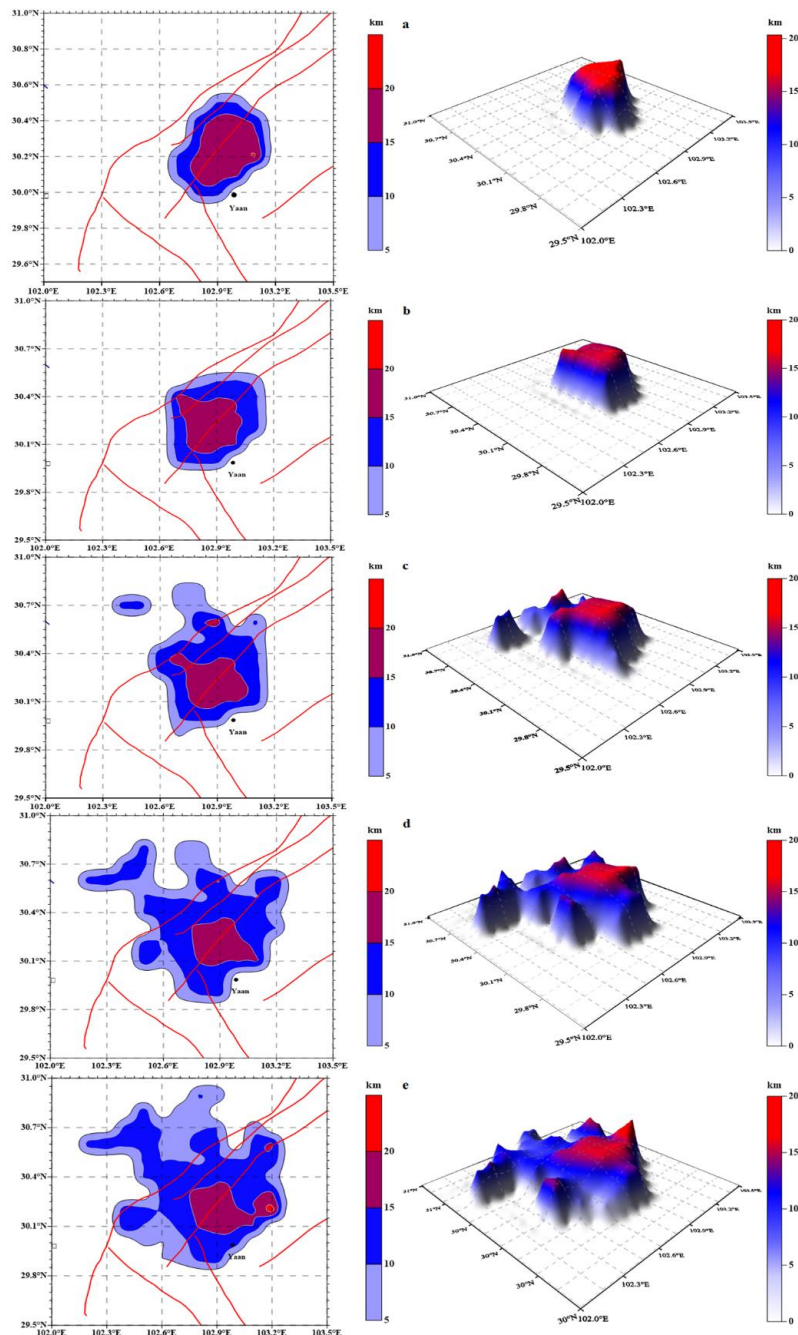
Figure 7. Spatial distribution of the focal depths of the aftershocks following the Lushan M_S 7.0 earthquake on the fault plane. Red lines represent the locations of faults. **a** One day after the mainshock; **b** 1 month after the mainshock; **c** 5 months after the mainshock; **d** 10 months after the mainshock; and **e** 2 years after the mainshock.

5 Discussion

Earthquake interaction can change the stress state of faults, which is reflected in both earthquake activity rate and earthquake size distribution. The relationship between stress state and b value can be used to quantify the effect of large earthquakes that can significantly change the stress states and, therefore, the earthquake size distribution. In contrast to previous studies on the Wenchuan and Lushan earthquakes, our paper focuses on a quantitative analysis and discussion of the effect of the Wenchuan M_S 8.0 and Lushan M_S 7.0 earthquakes on the size distribution of the earthquakes along the Longmenshan fault at different times.

Interpretation of the b value and its variability according to physical mechanisms has received considerable attention and discussion. In most cases, the observation of spatial and temporal b value variability can be caused by several factors: *i*) Process of estimation: homogeneity of catalog and method of calculation can affect the results. All the data in this work are from the Longmenshan fault and its surroundings, and each event includes the time, location and magnitude depth. The maximum likelihood estimation and least-squares regression method (Aki, 1965; Utsu, 1965; López-Pineda and Rebollar, 2005; Singh et al, 2011; Woessner et al. 2015; Shi et al.,2018, Li et al.,2018; Gulia and Wiemer, 2019) are used to estimate the b value and its uncertainty, but the latter is excessively affected by the largest earthquake magnitude. Marzocchi et al. (2020) measured the bias on b values caused by the magnitude binning and catalog incompleteness when the b value is estimated by the maximum likelihood estimation and provided guidance to reduce the likelihood of being misled by b value variation. *ii*) Stress conditions: the b value and its variation represent stress buildup and release. The differential stress is inversely dependent on the b value has been observed in laboratory experiments (Varotsos et al., 2013; Sarlis et al., 2013) as well as in the field (Scholz, 2015; Rodríguez-Pérez and Zuñiga, 2018). The stress acting on a fault may control the variation in the b value in space and time. Parsons et al. (2008) calculated the regional Coulomb stress changes on major faults surrounding the rupture resulting from the Wenchuan M_S 8.0 and showed that significant stress increased in the Lushan aftershock zone. Other studies obtained similar results (Shan et al., 2013; Parsons and Segou, 2014; Zhu, 2016). The spatial variation in the b values throughout the Lushan aftershock zone decreased after the M_S 8.0 mainshock (Fig. 5i), and the same effect occurred in the southern part of the Wenchuan aftershock zone after the M_S 7.0 event (Fig. 5g). These finding suggest that the b value is negatively correlated with stress and indicate the effect of the earthquakes interaction along the Longmenshan fault zone. *iii*) Crustal tectonics: the variation in b value can be interpreted according to the tectonic characteristics, i.e., rock heterogeneity (Gerstenberger et al., 2001), focal depth (Spada et al., 2013), pore pressure (Bachmann et al., 2012), and fault types (Schorlemmer et al., 2005; Gulia et al. 2010). Previous studies have shown that the b value in different types of faults is b(normal) > 1, b(strike-slip)~1, and b(thrust) < 1 (Beauval and Scotti, 2004; Ishibe et al., 2008; Gulia et al. 2010). As shown in the spatial footprints in Fig. 5, the b value of the southern part of the Longmenshan fault zone is lower than that in the northern part. This pattern is consistent with the tectonic characteristics of the Longmenshan fault, which is a strike-slip fault in the north and a thrust fault in the southern part (Hubbard and Shaw, 2009; Lei and Zhao, 2009).

Stress changes seem to be a key factor that affects the b value and its variation. Excepting the approach of estimation, all other factors are secondary because they are directly or indirectly

389   affected by the stress (El-Isa and Eaton, 2014). Therefore, the observed falls in the *b* values shown
390   in Fig. 5a and Fig. 5b was interpreted as changes in the related stress conditions, which could be
391   precursors to large earthquakes. However, these temporal variations may occur over a timescale
392   ranging from months to years, and the timeliness and effectiveness of this variability as an indicator
393   are difficult to guarantee. Additionally, there is usually an insufficient number of events to accurately
394   calculate the *b* value before large earthquakes. Gulia and Wiemer (2019) pointed out that the period
395   following a moderate earthquake is rich in such data, with thousands of events occurring within a
396   short period. These events may allow real-time monitoring of the evolution of *b* values. The authors
397   claim that the probability of a larger earthquake following a moderate earthquake increases by
398   several orders of magnitude if the *b* value remains the same or drops significantly rather than
399   increases. However, Brodsky (2019) suggested that the observed pattern revealing the changes in *b*
400   values is a statistical effect rather than deterministic and that researchers need more cases to test this
401   claim.

402   In general, thousands of aftershocks occur in the period following a large earthquake. Based
403   on these abundant data, there are two typically common operational aftershock forecasting models
404   used in aftershock hazard assessment, namely the short-term earthquake probability (STEP) model
405   (Gerstenberger et al., 2005) and epidemic-type aftershock sequence model (Ogata, 1988, 1999).
406   Gulia et al. (2018) reported that these models forecast a high probability for a repeat of the
407   mainshock rupture and thus substantially overestimate the aftershock hazard. This paradox can be
408   resolved by taking into account the stress changes and their effect on the earthquake size distribution.

409   Our results showed that the time series of the *b* value in the Longmenshan fault zone after the
410   mainshocks exhibited a period of significant fluctuation before returning to the stable state in both
411   the Wenchuan aftershock zone (one year) and the Lushan aftershock zone (ten months). Figure 6
412   and Figure 7 show that the time required for the *b* values to return to a stable state after both
413   mainshocks was entirely consistent with the time required for the aftershock depth images to cease
414   changing visibly. The spatial footprints of the changes in the *b* value reveal that the southern part of
415   the Longmenshan fault zone is lower than the northern part. This finding demonstrates that the
416   Wenchuan and Lushan events did not change the pattern of higher stress in the southern part of the
417   Longmenshan fault zone than in the northern part. However, the most obvious change is that after
418   the mainshock, the size distribution of the subsequent earthquakes in the Wenchuan source region
419   shifts toward relatively larger events (lower *b* values).

420   The Longmenshan fault zone began to develop in the Late Triassic, and severe tectonic
421   deformation occurred during the Indo-China and Himalayan movements, forming a combination of
422   thrust and strike-slip displacement (Lei and Zhao, 2009; Deng et al.,2012). Previous studies did not
423   comprehensively quantify the stable state for the Longmenshan fault zone before and after the two
424   large events in a long time series (Zhao et al. 2008; Wang et al., 2014; Parsons and Segou, 2014;
425   Zhu, 2016; Liu et al.,2017, Shi et al.,2018, Li et al.,2018). The *b* value is a measurable indicator of
426   earthquake size distribution within a specified region and period of time and is dependent on stress.
427   With our present results, we reported the temporal and spatial variation in *b* values before and after
428   two big earthquakes and fitted the source depth in time and space to quantify the stress changes and
429   their effect on the earthquake size distribution in the Longmenshan fault zone.

6 Conclusions

Based on the tectonic characteristics and potential seismicity surrounding the aftershock zones of the Wenchuan M_S 8.0 and Lushan M_S 7.0 earthquakes, we studied the spatial and temporal variation of b values in two source regions from 2000 to 2019. In addition, the spatial evolution process of the deep seismogenic environment in the Wenchuan and Lushan aftershock zones was drawn by spatial scanning and depth data fitting.

The results depict the decreasing trends of b values before the two large earthquakes in the study region. Additionally, the b value in the Wenchuan aftershock zone took approximately one year to enter a new stable state (b values ranging from 1.03 to 0.84), while the b value in the Lushan aftershock zone took approximately ten months to return to its original stable state (b=0.76). Moreover, the major aftershock active periods of the Wenchuan M_S 8.0 and Lushan M_S 7.0 earthquakes were less than one year and ten months, respectively, which are consistent with the time required for the b value to return to a stable state. The spatial footprints of the changes in the b values results reveal that the Wenchuan M_S 8.0 and Lushan M_S 7.0 events did not change the pattern of high b values in the north and low b values in the south along the Longmenshan fault zone.

We quantified the effect of the Wenchuan M_S 8.0 and Lushan M_S 7.0 earthquakes on the size distribution of earthquakes along the Longmenshan fault. Future studies can focus on how to quantify the effect of large earthquake size distribution across different tectonic regimes and apply the findings in potential seismic risk assessment.

Acknowledgments

This research was supported by the National Natural Science Foundation of China (Grant No. 41771537) and the Fundamental Research Funds for the Central Universities. The authors thank American Journal Experts (AJE) for polishing the language of this article. Datasets for this research are available in these in-text data citation references: Shi et al. (2018), [http://doi.org/10.6038/cjg2018M0024], Li et al. (2018), [http://doi.org/10.6038/cjg2018M0129] and China Earthquake Networks Center (CENC), [http://www.cenc.ac.cn/].

Author Contributions

Conceptualization, C X.C. and S.S.; Data curation, J.C.; Funding acquisition, C X.C.; Investigation, C.H. and S.S.; Methodology, C.H. and C X.C; Software and Code, C.H.; Manuscript editing, C.H.; Manuscript revision, C X.C. and P C.G.; Supervision, C X.C.; Visualization, J.Y. and M.Z.

Competing Interests

461

462 No conflicts of interest exist in the submission of this manuscript, and the manuscript is approved
463 by all authors for publication.

References

464

465 Akaike, H.: A new look at the statistical model identification, Ieee Transactions on Automatic
466 Control, AC19, 716-723, https://doi.org/10.1109/tac.1974.1100705, 1974.

467 Aki, K.: Maximum likelihood estimate of b in the formula log N= a-bM and its confidence limits,
468 Bull. Earthq. Res. Inst., Tokyo Univ., 43, 237-239, 1965.

469 Amitrano, D.: Brittle-ductile transition and associated seismicity: Experimental and numerical
470 studies and relationship with the b value, Journal Of Geophysical Research-Solid Earth, 108(B1),
471 2044, https://doi.org/10.1029/2001jb000680, 2003.

472 Bachmann, C. E., Wiemer, S., Goertz-Allmann, B. P., and Woessner, J.: Influence of pore-pressure
473 on the event-size distribution of induced earthquakes, Geophysical Research Letters, 39,
474 https://doi.org/10.1029/2012gl051480, 2012.

475 Beauval, C. and Scotti, O.: Quantifying sensitivities of PSHA for France to earthquake catalog
476 uncertainties, truncation of ground-motion variability, and magnitude limits, Bulletin Of the
477 Seismological Society Of America, 94(5), 1579-1594, https://doi.org/10.1785/012003246, 2004..

478 Brodsky, E. E.: Determining whether the worst earthquake has passed, Nature, 574, 185-186,
479 https://doi.org/10.1038/d41586-019-02972-z, 2019.

480 Delescluse, M., Chamot-Rooke, N., Cattin, R., Fleitout, L., Trubienko, O., and Vigny, C.: April 2012
481 intra-oceanic seismicity off Sumatra boosted by the Banda-Aceh megathrust, Nature, 490(7419),
482 240-244, https://doi.org/10.1038/nature11520, 2012.

483 Deng, B., Liu, S. G., Jansa, L., Cao, J. X., Cheng, Y., Li, Z. W., and Liu, S.: Sedimentary record of
484 Late Triassic transpressional tectonics of the Longmenshan thrust belt, SW China, Journal Of Asian
485 Earth Sciences, 48, 43-55, https://doi.org/10.1016/j.jseaes.2011.12.019, 2012.

486 DeVries, P. M. R., Viegas, F., Wattenberg, M., and Meade, B. J.: Deep learning of aftershock patterns
487 following large earthquakes, Nature, 560(7720), 632-634, https://doi.org/10.1038/s41586-018-
488 0438-y, 2018.

489 Du, F., Long, F., Ruan, X., Yi, G. X., Gong, Y., Zhao, M., Zhang, Z. W., Qiao, H. Z., Wang, Z., and
490 Wu, J.: The M7.0 Lushan earthquake and the relationship with the M8.0 Wenchuan earthquake in
491 Sichuan,   China,   Chinese   Journal   Of   Geophysics,   56(5),   1772-1783,

492   https://doi.org/10.6038/cjg20130535, 2013.

493   Durand, V., Bouchon, M., Karabulut, H., Marsan, D., and Schmittbuhl, J.: Link between Coulomb
494   stress changes and seismic activation in the eastern Marmara sea after the 1999, Izmit (Turkey),
495   earthquake, Journal Of Geophysical Research-Solid Earth, 118(2), 681-688, https://doi.org/
496   10.1002/jgrb.50077, 2013.

497   El-Isa, Z. H. and Eaton, D. W.: Spatiotemporal variations in the b-value of earthquake magnitude-
498   frequency   distributions: Classification   and   causes,   Tectonophysics,   615,   1-11,
499   https://doi.org/10.1016/j.tecto.2013.12.001, 2014.

500   Fang, L., Wu, J., Wang, W., Du, W., Su, J., Wang, C., Yang, T., and Cai, Y.: Aftershock Observation
501   and Analysis of the 2013 M-s 710 Lushan Earthquake, Seismological Research Letters, 86(4), 1135-
502   1142, https://doi.org/10.1785/0220140186, 2015.

503   Gerstenberger, M., Wiemer, S., and Giardini, D.: A systematic test of the hypothesis that the b value
504   varies   with   depth   in   California,   Geophysical   Research   Letters,   28(1),   57-60,
505   https://doi.org/10.1029/2000gl012026, 2001.

506   Gerstenberger, M. C., Wiemer, S., Jones, L. M., and Reasenberg, P. A.: Real-time forecasts of
507   tomorrow's   earthquakes   in   California,   Nature,   435(7040),   328-331,
508   https://doi.org/10.1038/nature03622, 2005.

509   Goebel, T. H. W., Schorlemmer, D., Becker, T. W., Dresen, G., and Sammis, C. G.: Acoustic
510   emissions document stress changes over many seismic cycles in stick-slip experiments, Geophysical
511   Research Letters, 40(10), 2049-2054, https://doi.org/10.1002/grl.50507, 2013.

512   Gulia, L., Rinaldi, A. P., Tormann, T., Vannucci, G., Enescu, B., and Wiemer, S.: The Effect of a
513   Mainshock on the Size Distribution of the Aftershocks, Geophysical Research Letters, 45(24),
514   13277-13287, https://doi.org/10.1029/2018gl080619, 2018.

515   Gulia, L. and Wiemer, S.: The influence of tectonic regimes on the earthquake size distribution: A
516   case study for Italy, Geophysical Research Letters, 37, https://doi.org/10.1029/2010gl043066, 2010.

517   Gulia, L. and Wiemer, S.: Real-time discrimination of earthquake foreshocks and aftershocks,
518   Nature, 574(7777), 193-199, https://doi.org/10.1038/s41586-019-1606-4, 2019.

519   Gutenberg, B. and Richter, C. F.: Frequency of earthquakes in California, Bulletin of the
520   Seismological society of America, 34(4), 185-188, 1944.

521   Ha, H., Olson, J. R., Bian, L., and Rogerson, P. A.: Analysis of Heavy Metal Sources in Soil Using
522   Kriging Interpolation on Principal Components, Environmental Science & Technology, 48(9), 4999-
523   5007, https://doi.org/10.1021/es405083f, 2014.

524   Huang, Q.: Seismicity changes prior to the M(s)8.0 Wenchuan earthquake in Sichuan, China,
525   Geophysical Research Letters, 35(23), https://doi.org/10.1029/2008gl036270, 2008.

526   Hubbard, J. and Shaw, J. H.: Uplift of the Longmen Shan and Tibetan plateau, and the 2008
527   Wenchuan (M=7.9) earthquake, Nature, 458(7235), 194-197, https://doi.org/10.1038/nature07837,
528   2009.

529   Jia, K., Zhou, S., Zhuang, J., and Jiang, C.: Possibility of the Independence between the 2013 Lushan
530   Earthquake and the 2008 Wenchuan Earthquake on Longmen Shan Fault, Sichuan, China,
531   Seismological Research Letters, 85(1), 60-67, https://doi.org/10.1785/0220130115, 2014.

532   Kilb, D., Gomberg, J., and Bodin, P.: Aftershock triggering by complete Coulomb stress changes,
533   Journal of Geophysical Research: Solid Earth, 107(B4), https://doi.org/10.1029/2001jb000202,
534   2002.

535   Lei, J. and Zhao, D.: Structural heterogeneity of the Longmenshan fault zone and the mechanism of
536   the 2008 Wenchuan earthquake (Ms 8.0), Geochemistry Geophysics Geosystems, 10(10),
537   https://doi.org/10.1029/2009gc002590, 2009.

538   Li, L., Adhikari, L. B., Li, G., and Gao, F. W.: Characteristics of temporal-spatial distribution of the
539   aftershocks of the 2008 M(s)8. 0 Wenchuan Earthquake, Chinese Journal Of Geophysics, 61(5),
540   1797-1805, https://doi.org/10.6038/cjg2018M0129, 2018.

541   Li, Y. Q., Jia, D., Wang, M. M., Shaw, J. H., He, J. K., Lin, A. M., Xiong, L., and Rao, G.: Structural
542   geometry of the source region for the 2013 Mw 6.6 Lushan earthquake: Implication for earthquake
543   hazard assessment along the Longmen Shan, Earth And Planetary Science Letters, 390, 275-286,
544   https://doi.org/10.1016/j.epsl.2014.01.018, 2014.

545   Liu, Y. B. and Pei, S. P.: Temporal and spatial variation of b-value before and after Wenchuan
546   earthquake and its tectonic implication, Chinese Journal Of Geophysics, 60(6), 2104-2112,
547   https://doi.org/10.6038/cjg20170607, 2017.

548   Lopez-Pineda, L. and Rebollar, C. J.: Source characteristics of the Mw 6.2 loreto earthquake of 12
549   March 2003 that occurred in a transform fault in the middle of the Gulf of California, Mexico,
550   Bulletin Of the Seismological Society Of America, 95(2), 419-430,
551   https://doi.org/10.1785/0120030227, 2005.

552   Mallman, E. P. and Zoback, M. D.: Assessing elastic Coulomb stress transfer models using
553   seismicity rates in southern California and southwestern Japan, Journal Of Geophysical Research-
554   Solid Earth, 112(B3), B03304, https://doi.org/10.1029/2005jb004076, 2007.

555   Marzocchi, W., Spassiani, I., Stallone, A., and Taroni, M.: How to be fooled searching for significant
556   variations of the b-value, Geophysical Journal International, 220(3), 1845-1856,
557   https://doi.org/10.1093/gji/ggz541, 2020.

558   McGrath, D., Zhang, C. S., and Carton, O. T.: Geostatistical analyses and hazard assessment on soil
559   lead in Silvermines area, Ireland, Environmental Pollution, 127(2), 239-248,
560   https://doi.org/10.1016/j.envpol.2003.07.002, 2004.

561   Mignan, A., Werner, M. J., Wiemer, S., Chen, C. C., and Wu, Y. M.: Bayesian Estimation of the

562   Spatially Varying Completeness Magnitude of Earthquake Catalogs, Bulletin Of the Seismological
563   Society Of America, 101(3), 1371-1385, https://doi.org/10.1785/0120100223, 2011.

564   Nanjo, K. Z., Hirata, N., Obara, K., and Kasahara, K.: Decade-scale decrease in b value prior to the
565   M9-class 2011 Tohoku and 2004 Sumatra quakes, Geophysical Research Letters, 39(20),
566   https://doi.org/10.1029/2012gl052997, 2012.

567   Nuannin, P., Kulhanek, O., and Persson, L.: Spatial and temporal b value anomalies preceding the
568   devastating off coast of NW Sumatra earthquake of December 26, 2004, Geophysical Research
569   Letters, 32(11), https://doi.org/10.1029/2005gl022679, 2005.

570   Ogata, Y.: Statistical models for earthquake occurrences and residual analysis for point processes,
571   Journal   of   the   American   Statistical   association,   83(401),   9-27,
572   https://doi.org/10.1080/01621459.1988.10478560, 1988.

573   Ogata, Y.: Space-time point-process models for earthquake occurrences, Annals Of the Institute Of
574   Statistical Mathematics, 50(2), 379-402, https://doi.org/10.1023/a:1003403601725, 1998.

575   Parsons, T., Ji, C., and Kirby, E.: Stress changes from the 2008 Wenchuan earthquake and increased
576   hazard in the Sichuan basin, Nature, 454(7203), 509-510, https://doi.org/10.1038/nature07177,
577   2008.

578   Parsons, T. and Segou, M.: Stress, Distance, Magnitude, and Clustering Influences on the Success
579   or Failure of an Aftershock Forecast: The 2013 M 6.6 Lushan Earthquake and Other Examples,
580   Seismological Research Letters, 85(1), 44-51, https://doi.org/10.1785/0220130100, 2014.

581   Rodriguez-Perez, Q. and Ramon Zuniga, F.: Imaging b-value depth variations within the Cocos and
582   Rivera   plates   at   the   Mexican   subduction   zone,   Tectonophysics,   734,   33-43,
583   https://doi.org/10.1016/j.tecto.2018.03.019, 2018.

584   Sarlis, N. V., Skordas, E. S., Varotsos, P. A., Nagao, T., Kamogawa, M., Tanaka, H., and Uyeda, S.:
585   Minimum of the order parameter fluctuations of seismicity before major earthquakes in Japan,
586   Proceedings   of   the   National   Academy   of   Sciences,   110(34),   13734-13738,
587   https://doi.org/10.1073/pnas.1312740110, 2013.

588   Scholz, C. H.: On the stress dependence of the earthquake b value, Geophysical Research Letters,
589   42(5), 1399-1402, https://doi.org/10.1002/2014gl062863, 2015.

590   Schorlemmer, D., Wiemer, S., and Wyss, M.: Variations in earthquake-size distribution across
591   different stress regimes, Nature, 437(7058), 539-542, https://doi.org/10.1038/nature04094, 2005.

592   Shan, B., Xiong, X., Zheng, Y., Jin, B., Liu, C., Xie, Z., and Hsu, H.: Stress changes on major faults
593   caused by 2013 Lushan earthquake and its relationship with 2008 Wenchuan earthquake, Science
594   China-Earth Sciences, 56(7), 1169-1176, https://doi.org/10.1007/s11430-013-4642-1, 2013.

595   Shi, H. X., Meng, L. Y., Zhang, X. M., Chang, Y., Yang, Z. T., Xie, W. Y., Hattori, K., and Han, P.:
596   Decrease in b value prior to the Wenchuan earthquake (M(s)8.0), Chinese Journal Of Geophysics,

597   61(5), 1874-1882, https://doi.org/10.6038/cjg2018M0024, 2018.

598   Singh, A. P., Mishra, O. P., Rastogi, B. K., and Kumar, D.: 3-D seismic structure of the Kachchh,
599   Gujarat, and its implications for the earthquake hazard mitigation, Natural Hazards, 57(1), 83-105,
600   https://doi.org/10.1007/s11069-010-9707-2, 2011.

601   Spada, M., Tormann, T., Wiemer, S., and Enescu, B.: Generic dependence of the frequency-size
602   distribution of earthquakes on depth and its relation to the strength profile of the crust, Geophysical
603   Research Letters, 40(4), 709-714, https://doi.org/10.1029/2012gl054198, 2013.

604   Stein, R. S., Barka, A. A., and Dieterich, J. H.: Progressive failure on the North Anatolian fault since
605   1939 by earthquake stress triggering, Geophysical Journal International, 128(3), 594-604,
606   https://doi.org/10.1111/j.1365-246X.1997.tb05321.x, 1997.

607   Sumy, D. F., Cochran, E. S., Keranen, K. M., Wei, M., and Abers, G. A.: Observations of static
608   Coulomb stress triggering of the November 2011 M5.7 Oklahoma earthquake sequence, Journal Of
609   Geophysical Research-Solid Earth, 119(3), 1904-1923, https://doi.org/10.1002/2013jb010612,
610   2014.

611   Toda, S., Stein, R. S., Beroza, G. C., and Marsan, D.: Aftershocks halted by static stress shadows,
612   Nature Geoscience, 5(6), 410-413, https://doi.org/10.1038/Ngeo1465, 2012.

613   Toda, S., Stein, R. S., and Lin, J.: Widespread seismicity excitation throughout central Japan
614   following the 2011 M=9.0 Tohoku earthquake and its interpretation by Coulomb stress transfer,
615   Geophysical Research Letters, 38(7), https://doi.org/10.1029/2011gl047834, 2011.

616   Tormann, T., Wiemer, S., and Mignan, A.: Systematic survey of high-resolution b value imaging
617   along Californian faults: Inference on asperities, Journal Of Geophysical Research-Solid Earth,
618   119(3), 2029-2054, https://doi.org/10.1002/2013jb010867, 2014.

619   Utsu, T.: A method for determining the value of" b" in a formula log n= a-bM showing the
620   magnitude-frequency relation for earthquakes, Geophys. Bull. Hokkaido Univ., 13, 99-103, 1965.

621   Utsu, T.: Representation and analysis of the earthquake size distribution: A historical review and
622   some new approaches, Pure And Applied Geophysics, 155, 509-535,
623   https://doi.org/10.1007/s000240050276, 1999.

624   Utsu, T., Ogata, Y., and Matsuura, R. S.: The Centenary Of the Omori Formula for a Decay Law Of
625   Aftershock Activity, Journal Of Physics Of the Earth, 43(1), 1-33, https://doi.org/
626   10.4294/jpe1952.43.1, 1995.

627   Varotsos, P. A., Sarlis, N. V., Skordas, E. S., and Lazaridou, M. S.: Seismic Electric Signals: An
628   additional fact showing their physical interconnection with seismicity, Tectonophysics, 589, 116-
629   125, https://doi.org/10.1016/j.tecto.2012.12.020, 2013.

630   Verdecchia, A., Pace, B., Visini, F., Scotti, O., Peruzza, L., and Benedetti, L.: The Role of
631   Viscoelastic Stress Transfer in Long-Term Earthquake Cascades: Insights After the Central Italy

632   2016-2017 Seismic Sequence, Tectonics, 37(10), 3411-3428, https://doi.org/10.1029/2018tc005110,
633   2018.

634   Wang, Y., Wang, F., Wang, M., Shen, Z.-K., and Wan, Y.: Coulomb Stress Change and Evolution
635   Induced by the 2008 Wenchuan Earthquake and its Delayed Triggering of the 2013 M-W 6.6 Lushan
636   Earthquake, Seismological Research Letters, 85(1), 52-59, https://doi.org/10.1785/0220130111,
637   2014.

638   Wech, A. G., Creager, K. C., Houston, H., and Vidale, J. E.: An earthquake-like magnitude-
639   frequency distribution of slow slip in northern Cascadia, Geophysical Research Letters, 37(22),
640   https://doi.org/10.1029/2010gl044881, 2010.

641   Wedmore, L. N. J., Walker, J. P. F., Roberts, G. P., Sammonds, P. R., McCaffrey, K. J. W., and Cowie,
642   P. A.: A 667 year record of coseismic and interseismic Coulomb stress changes in central Italy
643   reveals the role of fault interaction in controlling irregular earthquake recurrence intervals, Journal
644   Of Geophysical Research-Solid Earth, 122(7), 5691-5711, https://doi.org/10.1002/2017jb014054,
645   2017.

646   Woessner, J., Laurentiu, D., Giardini, D., Crowley, H., Cotton, F., Grunthal, G., Valensise, G.,
647   Arvidsson, R., Basili, R., Demircioglu, M. B., Hiemer, S., Meletti, C., Musson, R. W., Rovida, A.
648   N., Sesetyan, K., Stucchi, M., and Consortium, S.: The 2013 European Seismic Hazard Model: key
649   components and results, Bulletin Of Earthquake Engineering, 13(12), 3553-3596,
650   https://doi.org/10.1007/s10518-015-9795-1, 2015.

651   Woessner, J. and Wiemer, S.: Assessing the quality of earthquake catalogues: Estimating the
652   magnitude of completeness and its uncertainty, Bulletin Of the Seismological Society Of America,
653   95(2), 684-698, https://doi.org/10.1785/0120040007, 2005.

654   Zhang, S. J. and Zhou, S. Y.: Spatial and Temporal Variation of b-Values in Southwest China, Pure
655   And Applied Geophysics, 173(1), 85-96, https://doi.org/10.1007/s00024-015-1044-7, 2016.

656   Zhang, Y. Q., Dong, S. W., Hou, C. T., Shi, J. S., Wu, Z. H., Li, H. L., Sun, P., Liu, G., and Li, J.:
657   Seismogenic Structure of the April 20, 2013, Lushan Ms7 Earthquake in Sichuan, Acta Geol Sin-
658   Engl, 87(3), 633-645, https://doi.org/10.1111/1755-6724.12075, 2013.

659   Zhao, B. J., Yang, G. L., Wang, J. P., and Dong, F. F.: Research on b-Values Based on Fault Buffers,
660   Pure And Applied Geophysics, 177(1), 71-80, https://doi.org/10.1007/s00024-019-02163-x, 2020.

661   Zhao, Y. Z. and Wu, Z. L.: Mapping the b-values along the Longmenshan fault zone before and after
662   the 12 May 2008, Wenchuan, China, M-S 8.0 earthquake, Natural Hazards And Earth System
663   Sciences, 8(6), 1375-1385, https://doi.org/10.5194/nhess-8-1375-2008, 2008.

664   Zhu, S.: Is the 2013 Lushan earthquake (Mw=6.6) a strong aftershock of the 2008 Wenchuan, China
665   mainshock (Mw=7.9)?, Journal Of Geodynamics, 99, 16-26,
666   https://doi.org/10.1016/j.jog.2016.05.002, 2016.

667   Zuniga, F. R. and Wyss, M.: Most- and least-likely locations of large to great earthquakes along the

668   Pacific coast of Mexico estimated from local recurrence times based on b-values, Bulletin Of the
669   Seismological Society Of America, 91(6), 1717-1728, https://doi.org/10.1785/0120000303, 2001.
670